Fixed Switching Frequency Direct Model Predictive Control Based on Output Current Gradients

Petros Karamanakos*, Rasmus Mattila*, and Tobias Geyer†
*Faculty of Computing and Electrical Engineering, Tampere University of Technology, 33101 Tampere, Finland
Email: *p.karamanakos@ieee.org, rasmus.mattila@tut.fi
†ABB Corporate Research, 5405 Baden-Dättwil, Switzerland
Email: †t.geyer@ieee.org

***Abstract*—In this paper we present a direct model predictive control (MPC) scheme, which combines control and modulation in one computational stage. The MPC problem is formulated as a current control problem. By utilizing a fixed modulation cycle akin to pulse width modulation (PWM) that allows for one switching transition per phase and half-cycle a constant switching frequency and a discrete current harmonic spectrum result. Thus, the issues that relate to the variable switching frequency and current interharmonics of direct MPC schemes are resolved. To verify the effectiveness of the proposed method a variable speed drive system, which consists of a two-level voltage source inverter and a medium-voltage induction machine, serves as a case study.**

I. Introduction

The most utilized model predictive control (MPC) [1] strategy in power electronics is the so-called finite control set MPC (FCS-MPC) [2]. The output reference tracking and the modulation problem are formulated in one computational stage, i.e., akin to a direct control strategy [3]. The absence of the modulator, however, although it allows for fast transient responses, it comes with the pitfall of variable switching frequency and spread harmonic spectra [4]. Consequently, on the machine side of a variable speed drive, such harmonic current distortions can give rise to iron and copper losses and thus to thermal losses. When the grid-side converter is of concern, the relevant grid codes cannot be adhered to, rendering the implementation of such algorithms less effective.

Given the above, some attempts have been done to fix the issues related to the aforementioned problems of direct MPC. For example, some of them employ dead beat concepts to generate the reference signal that is fed into a modulator [5], [6]. By doing so, the behavior of the system is similar to that achieved with the modulator-based schemes. Therefore, on the one hand the aforementioned issues are fixed, but the transient response times get longer because of the modulator. Other techniques that have been proposed aim to include a "modulator" to the control scheme, with an eventual goal to reduce the ripples of the variables of interest, depending on the examined case study (e.g., output current, electromagnetic torque, flux, etc.), see, e.g., [7]–[11]. Such schemes allow for the converter switches to change state not only at the discrete time instants, but also at any instant within the sampling interval. Consequently, the switch positions that can potentially lead to high ripples are applied for less time than with conventional direct MPC schemes, resulting in an overall improved system performance. These techniques, however, can be either prone to suboptimality [7], [9]–[11] with spread harmonic spectra, or they fail to achieve constant switching frequency which affects the spectra in the expected way [8].

Further attempts to ensure a constant switching frequency in direct MPC schemes consider pre-computed switching sequences [12]–[14]. By utilizing such sequences the optimization problem reduces to the computation of the switching instants of the switching sequence. However, [12], [13] are limited to problems that are unconstrained with respect to time, implying that symmetry is not enforced in the implemented switching sequences, resulting in non-discrete harmonic spectra. Regarding [14], the algorithm is limited to simple, single-output systems, such as dc-dc converters.

To meet the control tasks of a fixed switching frequency and harmonic spectra with pronounced discrete harmonics as well as to keep the advantages of direct MPC (i.e., good tracking performance, fast transients), this paper proposes a direct MPC method that tackles the control problem from a different perspective. More specifically, the switch positions over one sampling interval are considered as known; the possible switching sequences are derived at each time step, rendering the switching time (i.e., the time instant a new switch position has to be applied to the plant) as the only optimization variable. By doing that, the multiobjective optimization problem is turned into one-objective, which means that there is no need for operation at the trade-off surfaces of the optimization variables. This implies that the problem is greatly simplified since no tuning is required, whereas optimality is guaranteed.

Moreover, by treating time as the sole optimization variable, the problem can be cast—as shown—as a quadratic program (QP) which is convex and, thus, easy to be solved. In addition, by allowing each phase to switch once within each sampling interval, a fixed switching frequency is guaranteed; this is determined by the chosen sampling interval. Finally, owing to the implicit presence of a modulator the dynamic behavior of the system is not deteriorated. The MPC problem, formulated as *constrained* optimization problem, allows for fast transients without violating the explicit time constraints. Consequently, operation at the physical limits of the plant is achieved while ensuring that the switching frequency remains constant.

To highlight the efficacy of the proposed direct MPC method, a variable speed drive system, consisting of a two-

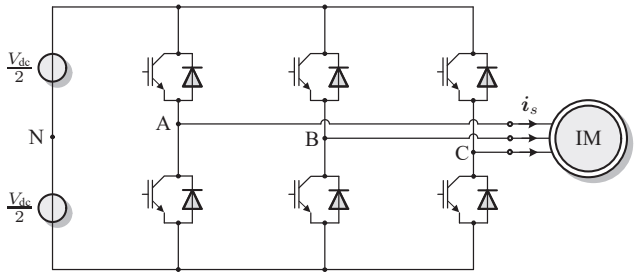

Fig. 1: Two-level three-phase voltage source inverter driving an induction motor (IM).

level voltage source inverter driving a medium-voltage (MV) induction machine (IM), is chosen as a case study. As it is shown, the stator current harmonic spectrum is comparable with that produced by carrier-based pulse width modulation (CB-PWM), while the very fast responses inherent to direct MPC are still present.

II. Problem Statement and Assumptions

The problem examined relates to the control of the stator current of an IM when driven by a two-level voltage source inverter with a constant dc-link voltage V_{dc} (Fig. 1). The mathematical model of the examined system and the formulation of the optimization problem are derived in the stationary orthogonal $\alpha\beta$ system. Therefore, the operation $\boldsymbol{\xi}_{\alpha\beta} = \boldsymbol{K}\boldsymbol{\xi}_{abc}$ is performed so as to map any variable in the abc plane $\boldsymbol{\xi}_{abc} = [\xi_a \ \xi_b \ \xi_c]^T$ into a two-dimensional vector $\boldsymbol{\xi}_{\alpha\beta} = [\xi_\alpha \ \xi_\beta]^T$ in the $\alpha\beta$ plane.

A. Control Model

The output potential of each phase of the two-level inverter can obtain two discrete voltage levels $-\frac{V_{\text{dc}}}{2}$ and $\frac{V_{\text{dc}}}{2}$, depending on the power switches position in the respective phase [15]. To model the switch position in phase $x \in \{a, b, c\}$ the variable $u_x \in \mathcal{U} = \{-1, 1\}$ is introduced. Based on this, the inverter output voltage—which is the voltage applied to the machine terminals $\boldsymbol{v}_{s,\alpha\beta}$—is[1]

$$\boldsymbol{v}_{\alpha\beta} = \frac{V_{\text{dc}}}{2}\,\boldsymbol{u}_{\alpha\beta} = \frac{V_{\text{dc}}}{2}\boldsymbol{K}\boldsymbol{u}\,. \tag{1}$$

Regarding the dynamics of the squirrel-cage IM, these can be fully described based on the stator current $\boldsymbol{i}_{s,\alpha\beta}$ and the rotor flux $\boldsymbol{\psi}_{r,\alpha\beta}$ as well as the angular speed of the rotor ω_r. Thus, the differential equations of interest are[2] [16]

$$\frac{\mathrm{d}\boldsymbol{i}_s}{\mathrm{d}t} = -\frac{1}{\tau_s}\boldsymbol{i}_s + \left(\frac{1}{\tau_r}\boldsymbol{I} - \omega_r \begin{bmatrix} 0 & -1 \\ 1 & 0 \end{bmatrix}\right)\frac{X_m}{\Phi}\boldsymbol{\psi}_r + \frac{X_r}{\Phi}\boldsymbol{v}_s \tag{2a}$$

$$\frac{\mathrm{d}\boldsymbol{\psi}_r}{\mathrm{d}t} = \frac{X_m}{\tau_r}\boldsymbol{i}_s - \frac{1}{\tau_r}\boldsymbol{\psi}_r + \omega_r \begin{bmatrix} 0 & -1 \\ 1 & 0 \end{bmatrix}\boldsymbol{\psi}_r \tag{2b}$$

$$\frac{\mathrm{d}\omega_r}{\mathrm{d}t} = \frac{1}{H}(T_e - T_\ell)\,, \tag{2c}$$

[1]Vectors in the $\alpha\beta$ plane are denoted with the corresponding subscript. For vectors in the abc plane the subscript is omitted.

[2]For notational convenience the subscript $\alpha\beta$ is dropped from $\boldsymbol{i}_s$, $\boldsymbol{\psi}_r$ and $\boldsymbol{v}_s$ in (2).

where R_s (R_r) is the stator (rotor) resistance, X_{ls} (X_{lr}) and X_m the stator (rotor) leakage and mutual reactances, respectively, H denotes the moment of inertia, and T_ℓ the mechanical load torque. Moreover, $\tau_s = X_r\Phi/(R_sX_r^2 + R_rX_m^2)$ and $\tau_r = X_r/R_r$ are the stator and rotor time constants, respectively, while the constant Φ is defined as $\Phi = X_sX_r - X_m^2$, with $X_s = X_{ls} + X_m$ and $X_r = X_{lr} + X_m$. Finally, T_e is the electromagnetic torque, and $\boldsymbol{I}$ is the identity matrix of appropriate dimension (here two-dimensional).

Given (2), the discrete-time state-space model of the drive used by the to-be-developed MPC algorithm is of the form

$$\boldsymbol{x}(k+1) = \boldsymbol{A}\boldsymbol{x}(k) + \boldsymbol{B}\boldsymbol{u}(k) \tag{3a}$$

$$\boldsymbol{y}(k) = \boldsymbol{C}\boldsymbol{x}(k)\,, \tag{3b}$$

where the stator current and the rotor flux in the $\alpha\beta$ plane constitute the state vector $\boldsymbol{x} = [i_{s\alpha} \ i_{s\beta} \ \psi_{r\alpha} \ \psi_{r\beta}]^T$, whereas the stator current is the output variable, i.e., $\boldsymbol{y} = \boldsymbol{i}_{s,\alpha\beta}$. Finally, the three-phase switch position $\boldsymbol{u} = [u_a \ u_b \ u_c]^T \in \boldsymbol{\mathcal{U}} = \mathcal{U} \times \mathcal{U} \times \mathcal{U} = \mathcal{U}^3$ forms the input vector. The matrices $\boldsymbol{A}$ and $\boldsymbol{B}$ are calculated using exact discretization, i.e., they are of the form $\boldsymbol{A} = \mathbf{e}^{\boldsymbol{F}T_s}$ and $\boldsymbol{B} = -\boldsymbol{F}^{-1}(\boldsymbol{I} - \boldsymbol{A})\boldsymbol{G}$, where $\boldsymbol{F}$ and $\boldsymbol{G}$ are the continuous-time matrices which can be easily derived based on (2) [3]. $\boldsymbol{I}$ is the identity matrix, $\mathbf{e}$ the matrix exponential, T_s the sampling interval, and $k \in \mathbb{N}$.

B. Control Problem

The goal of the proposed approach is to minimize the stator current ripple while keeping the switching frequency of the inverter constant. To do so, the converter switches are allowed to change state within the sampling interval T_s rather than only at the discrete time steps $k, k+1, \ldots$. Moreover, to guarantee equal load distribution among the three phases, all three phases have to switch once within each T_s.

To achieve the aforementioned control objectives, the objective function could take into account the (squared) rms error of the stator current, i.e.,

$$\begin{aligned} J &= \frac{1}{T_s}\int_0^{T_s} \big(\boldsymbol{i}_{s,\text{ref},\alpha\beta}(t) - \boldsymbol{i}_{s,\alpha\beta}(t)\big)^T \big(\boldsymbol{i}_{s,\text{ref},\alpha\beta}(t) - \boldsymbol{i}_{s,\alpha\beta}(t)\big)\,\mathrm{d}t \\ &= \frac{1}{T_s}\int_0^{T_s} ||\boldsymbol{i}_{s,\text{ref},\alpha\beta}(t) - \boldsymbol{i}_{s,\alpha\beta}(t)||_2^2\,\mathrm{d}t\,, \end{aligned} \tag{4}$$

where $\boldsymbol{i}_{s,\text{ref},\alpha\beta}$ is the stator current reference. Owing to the Parseval theorem, minimizing (4) is equivalent to minimizing the squared total harmonic distortion (THD) of the current over the sampling interval.

We introduce the switching instants t_z, $z \in \{1, 2, 3\}$. These switching instants occur consecutively within the sampling interval, i.e., we impose $0 < t_1 < t_2 < t_3 < T_s$. Assume that the switch position $\boldsymbol{u}(t_0^-)$ was applied at the end of the last sampling interval. At the beginning of the current sampling interval, at $t_0 \equiv 0$, it therefore holds that $\boldsymbol{u}(t_0) = \boldsymbol{u}(t_0^-)$. At time instant t_1 the switch position changes from $\boldsymbol{u}(t_0)$ to $\boldsymbol{u}(t_1)$. Similar statements can be made for the time instants

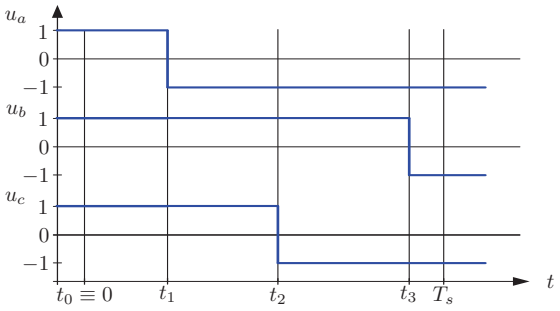

(a) Three-phase switch position

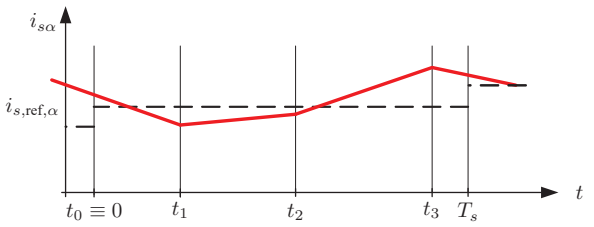

(b) Stator current (α-component)

Fig. 2: Evolution of i_{sa} within one T_s by applying the depicted switching sequence, assuming $\boldsymbol{u}(t_0^-) = \boldsymbol{u}(t_0) = [1\ 1\ 1]^T$ and the phase sequence $a \rightarrow c \rightarrow b$.

TABLE I: Possible sequences for the single-phase switch transitions

Phases to switch		
First	Second	Third
a	b	c
a	c	b
b	a	c
b	c	a
c	a	b
c	b	a

t_2 and t_3. We define the vector of switching times $\boldsymbol{t}$ and the vector of switch positions (the switching sequence) $\boldsymbol{U}$ as

$$\boldsymbol{t} = [t_1\ t_2\ t_3]^T \tag{5a}$$

$$\boldsymbol{U} = [\boldsymbol{u}^T(t_0)\ \boldsymbol{u}^T(t_1)\ \boldsymbol{u}^T(t_2)\ \boldsymbol{u}^T(t_3)]^T\,. \tag{5b}$$

Example 1: *Consider the drive system in Fig. 1, and assume that $\boldsymbol{u}(t_0^-) = [1\ 1\ 1]^T$ was applied at the end of the previous sampling interval, as depicted in Fig. 2. In the current sampling interval, the switch positions $\boldsymbol{u}(t_1) = [-1\ 1\ 1]^T$, $\boldsymbol{u}(t_2) = [-1\ 1\ -1]^T$, and $\boldsymbol{u}(t_3) = [-1\ -1\ -1]^T$ are applied to the converter at the time instants t_1, t_2 and t_3, respectively. In doing so, the evolution of the stator current is controlled, as shown in Fig. 2, where it is depicted along with its reference value.*

The switching instants divide the interval $[0, T_s)$ in (4) into the four subintervals $[0, t_1)$, $[t_1, t_2)$, $[t_2, t_3)$, and $[t_4, T_s)$. The three phases can switch in six different chronological orders, as summarized in Table I. To better understand this concept, the following example is provided.

Example 2: *For $\boldsymbol{u}(t_0) = \boldsymbol{u}(t_0^-) = [1\ 1\ 1]^T$ and the phase sequence $a \rightarrow b \rightarrow c$, the sequence of the to-be-applied three-phase switch positions is:*

$$\begin{aligned}
\boldsymbol{u}(t_0) &= [\ \ 1\ \ \ 1\ \ \ 1]^T\,,\ t_0 \leq t < t_1\\
\boldsymbol{u}(t_1) &= [-1\ \ \ 1\ \ \ 1]^T\,,\ t_1 \leq t < t_2\\
\boldsymbol{u}(t_2) &= [-1\ -1\ \ \ 1]^T\,,\ t_2 \leq t < t_3\\
\boldsymbol{u}(t_3) &= [-1\ -1\ -1]^T\,,\ t_3 \leq t < T_s\,.
\end{aligned}$$

For the phase sequence $a \rightarrow c \rightarrow b$, which is shown in Fig. 2(a), the switching sequence becomes

$$\begin{aligned}
\boldsymbol{u}(t_0) &= [\ \ 1\ \ \ 1\ \ \ 1]^T\,,\ t_0 \leq t < t_1\\
\boldsymbol{u}(t_1) &= [-1\ \ \ 1\ \ \ 1]^T\,,\ t_1 \leq t < t_2\\
\boldsymbol{u}(t_2) &= [-1\ \ \ 1\ -1]^T\,,\ t_2 \leq t < t_3\\
\boldsymbol{u}(t_3) &= [-1\ -1\ -1]^T\,,\ t_3 \leq t < T_s\,.
\end{aligned}$$

The same logic applies to the remaining four combinations.

III. Control Method

For the proposed control algorithm two assumptions are made. First, the variable of interest (i.e., stator current) evolves linearly over one T_s, i.e., its gradient remains constant. This simplification is valid since $T_s \ll T_1$, with T_1 being the fundamental period. Second, the reference of the stator current is constant over the same time interval.

A. Stator Current Gradients

Given the aforementioned assumptions, the evolution of the stator current within the four subintervals can be described by its corresponding gradient $\boldsymbol{m} = \frac{\mathrm{d}\boldsymbol{i}_{s,\alpha\beta}(t)}{\mathrm{d}t} \in \mathbb{R}^2$ as follows:

1) $t_0 \leq t < t_1$: At the beginning of the sampling interval ($t_0 \equiv 0$) the three-phase switch position applied in the previous T_s is applied to the plant, i.e., $\boldsymbol{u}(t_0) = \boldsymbol{u}(t_0^-)$. Consequently, the current evolves with the gradient $\boldsymbol{m}(t_0) = \boldsymbol{i}_{s,\alpha\beta}(t_0) + \boldsymbol{C}\boldsymbol{G}\boldsymbol{u}(t_0)$.
2) $t_1 \leq t < t_2$: At instant t_1 a new three-phase switch position $\boldsymbol{u}(t_1)$ is applied that allows for one commutation in one of the three phases, i.e., $||\boldsymbol{u}(t_1) - \boldsymbol{u}(t_0)||_1 = 2$. As a result, the current evolves with the gradient $\boldsymbol{m}(t_1) = \boldsymbol{i}_{s,\alpha\beta}(t_0) + \boldsymbol{C}\boldsymbol{G}\boldsymbol{u}(t_1)$. Note that the gradient at time instant t_1 depends on the current at time instant t_0 (rather than at t_1) because of the assumption made above that the gradients are constant within the sampling interval.
3) $t_2 \leq t < t_3$: At instant t_2 the three-phase switch position $\boldsymbol{u}(t_2)$ is applied that allows for one commutation in one of the remaining two phases, i.e., $||\boldsymbol{u}(t_2) - \boldsymbol{u}(t_1)||_1 = 2$ and $||\boldsymbol{u}(t_2) - \boldsymbol{u}(t_0)||_1 = 4$. The current evolves with the gradient $\boldsymbol{m}(t_2) = \boldsymbol{i}_{s,\alpha\beta}(t_0) + \boldsymbol{C}\boldsymbol{G}\boldsymbol{u}(t_2)$.
4) $t_3 \leq t < T_s$: For the last interval a switch position $\boldsymbol{u}(t_3)$ is implemented that allows for one commutation in the last phase that has been inactive thus far, i.e., $||\boldsymbol{u}(t_3) - \boldsymbol{u}(t_2)||_1 = 2$ and $||\boldsymbol{u}(t_3) - \boldsymbol{u}(t_0)||_1 = 6$. The current evolves with the gradient $\boldsymbol{m}(t_3) = \boldsymbol{i}_{s,\alpha\beta}(t_0) + \boldsymbol{C}\boldsymbol{G}\boldsymbol{u}(t_3)$.

B. Objective function

To make the control problem computationally tractable, we simplify it in three steps. First, we apply the assumptions made at the beginning of Section III. This turns the objective function into a cubic function of the time instants t_1, t_2 and t_3. As this problem is nonconvex, another simplification is required. Rather than capturing the rms deviation of the controlled quantities from their references, we penalize in the objective function the sampled squared error. This simplification turns the objective function into a quadratic function of time. Provided that a sufficiently large number of regularly spaced samples is used within the sampling interval, this simplification approximates the rms error accurately.

Introducing regularly spaced samples, however, results in numerous combinations between sub-sampling interval and switching instant, making this approach impractical. Therefore, in a third step, we limit ourselves to a few irregularly spaced samples. In the simplest case, the deviation of the controlled variables from their references is penalized only at the time instants t_1, t_2, t_3 and T_s. This is a fairly coarse approximation of the rms error, which is nevertheless often quite effective.

In light of these three simplification steps, the objective function (4) is written as

$$\begin{aligned} J = {} & ||\boldsymbol{i}_{s,\mathrm{ref},\alpha\beta} - \boldsymbol{i}_{s,\alpha\beta}(t_1)||_2^2 + ||\boldsymbol{i}_{s,\mathrm{ref},\alpha\beta} - \boldsymbol{i}_{s,\alpha\beta}(t_2)||_2^2 \\ & + ||\boldsymbol{i}_{s,\mathrm{ref},\alpha\beta} - \boldsymbol{i}_{s,\alpha\beta}(t_3)||_2^2 + ||\boldsymbol{i}_{s,\mathrm{ref},\alpha\beta} - \boldsymbol{i}_{s,\alpha\beta}(T_s)||_2^2 , \end{aligned} \tag{6}$$

where $\boldsymbol{i}_{s,\mathrm{ref},\alpha\beta} = \boldsymbol{i}_{s,\mathrm{ref},\alpha\beta}(t_0)$ and

$$\boldsymbol{i}_{s,\alpha\beta}(t_1) = \boldsymbol{i}_{s,\alpha\beta}(t_0) + \boldsymbol{m}(t_0)\, t_1 \tag{7a}$$

$$\begin{aligned} \boldsymbol{i}_{s,\alpha\beta}(t_2) &= \boldsymbol{i}_{s,\alpha\beta}(t_1) + \boldsymbol{m}(t_1)\,(t_2 - t_1) \\ &= \boldsymbol{i}_{s,\alpha\beta}(t_0) + \boldsymbol{m}_0\, t_1 + \boldsymbol{m}(t_1)\, t_2 \end{aligned} \tag{7b}$$

$$\begin{aligned} \boldsymbol{i}_{s,\alpha\beta}(t_3) &= \boldsymbol{i}_{s,\alpha\beta}(t_2) + \boldsymbol{m}(t_2)\,(t_3 - t_2) \\ &= \boldsymbol{i}_{s,\alpha\beta}(t_0) + \boldsymbol{m}_0\, t_1 + \boldsymbol{m}_1\, t_2 + \boldsymbol{m}(t_2)\, t_3 \end{aligned} \tag{7c}$$

$$\begin{aligned} \boldsymbol{i}_{s,\alpha\beta}(T_s) &= \boldsymbol{i}_{s,\alpha\beta}(t_3) + \boldsymbol{m}(t_3)\,(T_s - t_3) \\ &= \boldsymbol{i}_{s,\alpha\beta}(t_0) + \boldsymbol{m}_0\, t_1 + \boldsymbol{m}_1\, t_2 + \boldsymbol{m}_2\, t_3 + \boldsymbol{m}(t_3)\, T_s, \end{aligned} \tag{7d}$$

with $\boldsymbol{m}_0 = \boldsymbol{m}(t_0) - \boldsymbol{m}(t_1)$, $\boldsymbol{m}_1 = \boldsymbol{m}(t_1) - \boldsymbol{m}(t_2)$ and $\boldsymbol{m}_2 = \boldsymbol{m}(t_2) - \boldsymbol{m}(t_3)$. Thus, function (6) in vector form becomes

$$J = \left\| \underbrace{\begin{bmatrix} \boldsymbol{i}_{s,\mathrm{err},\alpha\beta}(t_0) \\ \boldsymbol{i}_{s,\mathrm{err},\alpha\beta}(t_0) \\ \boldsymbol{i}_{s,\mathrm{err},\alpha\beta}(t_0) \\ \boldsymbol{i}'_{s,\mathrm{err},\alpha\beta}(t_0) \end{bmatrix}}_{\boldsymbol{r}} - \underbrace{\begin{bmatrix} \boldsymbol{m}(t_0) & \boldsymbol{0} & \boldsymbol{0} \\ \boldsymbol{m}_0 & \boldsymbol{m}(t_1) & \boldsymbol{0} \\ \boldsymbol{m}_0 & \boldsymbol{m}_1 & \boldsymbol{m}(t_2) \\ \boldsymbol{m}_0 & \boldsymbol{m}_1 & \boldsymbol{m}_2 \end{bmatrix}}_{\boldsymbol{M}} \underbrace{\begin{bmatrix} t_1 \\ t_2 \\ t_3 \end{bmatrix}}_{\boldsymbol{t}} \right\|_2^2 , \tag{8}$$

where $\boldsymbol{i}_{s,\mathrm{err},\alpha\beta}(t_0) = \boldsymbol{i}_{s,\mathrm{ref},\alpha\beta} - \boldsymbol{i}_{s,\alpha\beta}(t_0)$, $\boldsymbol{i}'_{s,\mathrm{err},\alpha\beta}(t_0) = \boldsymbol{i}_{s,\mathrm{err},\alpha\beta}(t_0) - \boldsymbol{m}(t_3)T_s$ and $\boldsymbol{0}$ is the two-dimensional zero vector.

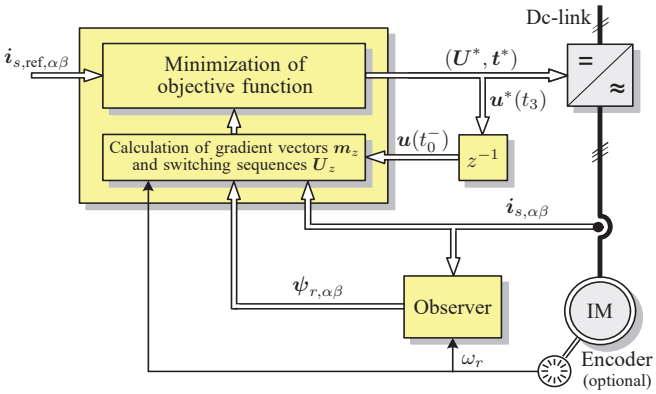

Fig. 3: Direct model predictive current control with fixed switching frequency for the three-phase two-level inverter with an induction machine.

Algorithm 1 Direct MPC with fixed switching frequency

Given $\boldsymbol{u}(t_0^-)$, $\boldsymbol{i}_{s,\mathrm{ref},\alpha\beta}(t_0)$ and $\boldsymbol{i}_{s,\alpha\beta}(t_0)$

0. Compute the corresponding gradient vectors $\boldsymbol{m}_z$, $z \in \{0, 1, \ldots, 6\}$.
1. Enumerate the possible $\boldsymbol{U}_z$, $z \in \{1, 2, \ldots, 6\}$, starting from $\boldsymbol{u}(t_0^-)$.
2. For each $\boldsymbol{U}_z$: Solve the QP (10). This yields $\boldsymbol{t}_z$ and J_z.
3. Solve the trivial optimization problem (11). This yields $\boldsymbol{t}^*$ and $\boldsymbol{U}^*$.

Return $\boldsymbol{t}^*$ and $\boldsymbol{U}^*$.

C. Control Algorithm

In a pre-processing step, the possible stator current gradients that depend on the measured current $\boldsymbol{i}_{s,\alpha\beta}(t_0)$ and the possible switch positions $\boldsymbol{u}$ of the power converter are computed. In the case of a two-level converter, seven switch positions $\boldsymbol{u}$ yield different voltage vectors in the $\alpha\beta$ plane, which result in the seven unique gradients $\boldsymbol{m}_z$, with $z \in \{0, 1, \ldots, 6\}$. To compute these gradients, we use the expression

$$\boldsymbol{m}_z = \boldsymbol{i}_{s,\alpha\beta}(t_0) + \boldsymbol{C}\boldsymbol{G}\boldsymbol{u}_{z,\alpha\beta} , \tag{9}$$

where $\boldsymbol{u}_{z,\alpha\beta}$ refers to the seven different switch positions in the $\alpha\beta$ plane.

In a first step, depending on the previously applied switch position $\boldsymbol{u}(t_0^-)$, the control algorithm enumerates the corresponding six switching sequences $\boldsymbol{U}_z$, $z \in \{1, 2, \ldots, 6\}$, see Table I.

In a second step, the first switching sequence $\boldsymbol{U}_1$ is considered and an optimization problem can be solved. With the simplified objective function (8), this optimization problem takes the form

$$\begin{aligned} \underset{\boldsymbol{t} \in \mathbb{R}^3}{\text{minimize}} \quad & ||\boldsymbol{r} - \boldsymbol{M}\boldsymbol{t}||_2^2 \\ \text{subject to} \quad & 0 < t_1 < t_2 < t_3 < T_s . \end{aligned} \tag{10}$$

Problem (10) is a convex QP, which can be easily solved. Its solution (the so-called optimizer) is the vector of switching instants $\boldsymbol{t}_1$ for the switching sequence $\boldsymbol{U}_1$. The same problem is solved for the remaining five switching sequences. This leads to the six triplets of switching instants $\boldsymbol{t}_z$, switching sequences $\boldsymbol{U}_z$ and values of the objective function J_z, with $z \in \{1, 2, \ldots, 6\}$.

In a third and last step, the triplet is chosen with the minimal value of the objective function. Specifically, the trivial problem

$$\underset{z}{\text{minimize}}\ J_z \tag{11}$$

is solved to determine the optimal triplet of switching instants $\boldsymbol{t}^* = [t_1^*\ t_2^*\ t_3^*]^T$, switching sequence $\boldsymbol{U}^* = [\boldsymbol{u}^{*T}(t_0)\ \boldsymbol{u}^{*T}(t_1)\ \boldsymbol{u}^{*T}(t_2)\ \boldsymbol{u}^{*T}(t_3)]^T$ and value of the objective function J^*. The resulting optimal switching sequence is applied with the appropriate switching times to the converter. The block diagram of the proposed direct MPC scheme is shown in Fig. 3. The pseudocode of the control method is summarized as Algorithm 1.

IV. Performance Evaluation

The presented simulation results were obtained based on an MV drive (Fig. 1) consisting of a squirrel cage IM with $3.3\,\text{kV}$ rated voltage, $356\,\text{A}$ rated current, $2\,\text{MVA}$ rated power, $50\,\text{Hz}$ nominal frequency, 0.25 p.u. total leakage inductance, and a two-level voltage source inverter with the constant dc-link voltage $V_{\text{dc}} = 5.2\,\text{kV}$. The sampling interval was set to $T_s = 476.2\,\mu\text{s}$ so that a (constant) switching frequency of $1{,}050\,\text{Hz}$ results. All results are shown in the p.u. system.

The steady-state performance of the drive is shown in Fig. 4. As can be seen in Fig. 4(a), the three-phase stator current waveforms—illustrated over one fundamental period—accurately track their references. The resulting current spectrum is shown in Fig. 4(b). Current harmonics are located only at odd and non-triplen integer multiples of the fundamental frequency. The THD, which quantifies the current tracking performance of the controller and the in-built modulation, is 7.17%. Fig. 4(c) shows the three-phase switch positions. For comparison purposes, a linear controller with CB-PWM and third harmonic injection was implemented. The results shown in Fig. 5 are similar to those of the direct MPC scheme. The current THD is with 7.34% slightly worse than that of direct MPC. The current harmonics are located at the same odd and non-triplen integer multiples of the fundamental frequency. However, the magnitudes of the low-order current harmonics differ. For direct MPC, the 5^{th} and 7^{th} harmonics are pronounced. Methods on how to reduce these low-frequency harmonics are presently under study.

Figs. 6 and 7 compare the performance of the two schemes during transients. While operating at nominal speed, reference torque steps of magnitude $1\,\text{p.u.}$ are imposed. The torque reference is translated into a corresponding stator current reference according to the principle of field-oriented control. For the proposed direct MPC, the stator currents in Fig. 6(a) accurately track their new references. The semiconductor switches are operated such that the available dc-link voltage is fully utilized, see Fig. 6(c). Therefore, the settling time is limited only by the available dc-link voltage. We conclude that the proposed controller inherits the favorable dynamic behavior that characterizes direct MPC schemes by removing the torque error as quickly as possible. To do so, the drive system is operated at its physical limit. As is to be expected, the dynamic performance of the modulator-based scheme with proportional-integral (PI) current controllers is slightly slower, as shown in Fig. 7.

V. Conclusions

In this paper we proposed a direct MPC method that achieves a fixed switching frequency and minimizes the stator current error. To this end, the gradient of the stator current is taken into account to compute the so-called switching times within the sampling interval. Moreover, by allowing for one switching transition per phase within each sampling interval, the symmetries in the switching patterns observed in modulator-based schemes appear. As a result, interharmonics are eliminated and discrete harmonics at integer multiples of the fundamental frequency are pronounced. As shown, when a drive system consisting of a two-level inverter and an induction machine is taken into account, the proposed direct MPC exhibits a similar steady-state behavior as a linear controller with CB-PWM, whereas it has a better dynamic behavior which approaches that of a deadbeat controller.

It is important to highlight that the main benefit of the proposed method is the fixed modulation interval combined with the high controller bandwidth. The latter is up to three times higher than that of indirect control methods, such as standard field-oriented control with CB-PWM. This characteristic is expected to make a difference when considering more complicated systems, such as converters with LC filters. Such research is ongoing and the promising results will be published soon. Moreover, future work relates to the elimination of the low frequency harmonics, as observed in Fig. 4(b). Refinements, including longer prediction horizons, more intermediate samples to better approximate the rms error, etc., will be examined and evaluated.

References

[1] J. B. Rawlings and D. Q. Mayne, *Model Predictive Control: Theory and Design*. Madison, WI: Nob Hill, 2009.

[2] P. Cortés, M. P. Kazmierkowski, R. M. Kennel, D. E. Quevedo, and J. Rodríguez, "Predictive control in power electronics and drives," *IEEE Trans. Ind. Electron.*, vol. 55, no. 12, pp. 4312–4324, Dec. 2008.

[3] T. Geyer, *Model predictive control of high power converters and industrial drives*. Hoboken, NJ: Wiley, 2016.

[4] ——, "A comparison of control and modulation schemes for medium-voltage drives: Emerging predictive control concepts versus PWM-based schemes," *IEEE Trans. Ind. Appl.*, vol. 47, no. 3, pp. 1380–1389, May/Jun. 2011.

[5] A. Bouafia, J.-P. Gaubert, and F. Krim, "Predictive direct power control of three-phase pulsewidth modulation (PWM) rectifier using space-vector modulation (SVM)," *IEEE Trans. Power Electron.*, vol. 25, no. 1, pp. 228–236, Jan. 2010.

[6] R. O. Ramírez, J. R. Espinoza, F. Villarroel, E. Maurelia, and M. E. Reyes, "A novel hybrid finite control set model predictive control scheme with reduced switching," *IEEE Trans. Ind. Electron.*, vol. 61, no. 11, pp. 5912–5920, Nov. 2014.

[7] Y. Zhang, W. Xie, Z. Li, and Y. Zhang, "Low-complexity model predictive power control: Double-vector-based approach," *IEEE Trans. Ind. Electron.*, vol. 61, no. 11, pp. 5871–5880, Nov. 2014.

[8] P. Karamanakos, P. Stolze, R. M. Kennel, S. Manias, and H. du T. Mouton, "Variable switching point predictive torque control of induction machines," *IEEE J. Emerg. Sel. Topics Power Electron.*, vol. 2, no. 2, pp. 285–295, Jun. 2014.

[9] L. Tarisciotti, P. Zanchetta, A. Watson, S. Bifaretti, and J. C. Clare, "Modulated model predictive control for a seven-level cascaded H-bridge back-to-back converter," *IEEE Trans. Ind. Electron.*, vol. 61, no. 10, pp. 5375–5383, Oct. 2014.

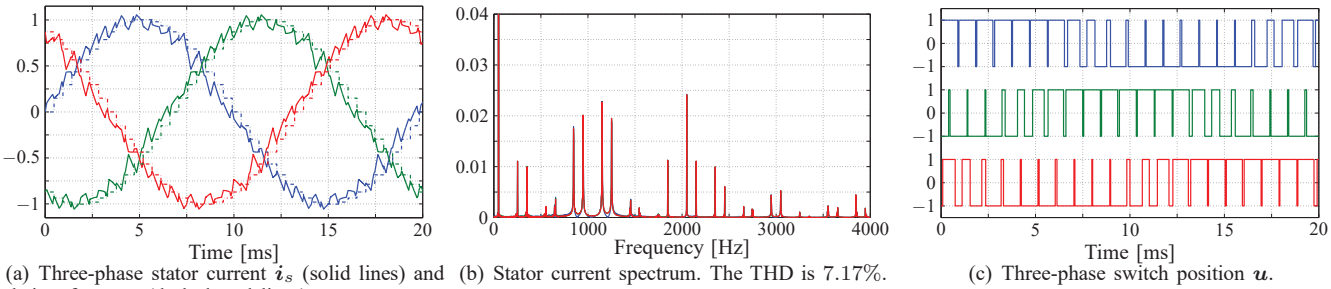

(a) Three-phase stator current $\boldsymbol{i}_s$ (solid lines) and their references (dash-dotted lines). (b) Stator current spectrum. The THD is 7.17%. (c) Three-phase switch position $\boldsymbol{u}$.

Fig. 4: Simulated waveforms produced by the proposed direct model predictive control with current reference tracking at steady-state operation, at full speed and rated torque. The switching frequency is 1050 Hz.

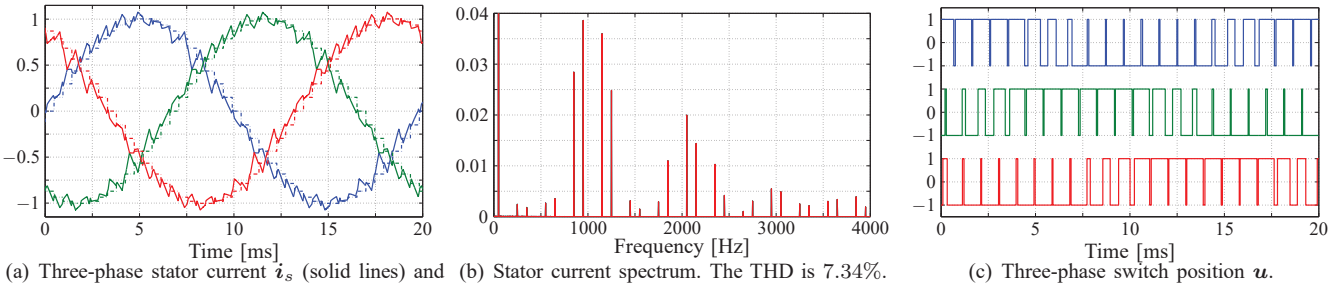

(a) Three-phase stator current $\boldsymbol{i}_s$ (solid lines) and their references (dash-dotted lines). (b) Stator current spectrum. The THD is 7.34%. (c) Three-phase switch position $\boldsymbol{u}$.

Fig. 5: Simulated waveforms produced by the CB-PWM with third harmonic injection at steady-state operation, at full speed and rated torque. The switching frequency is 1050 Hz.

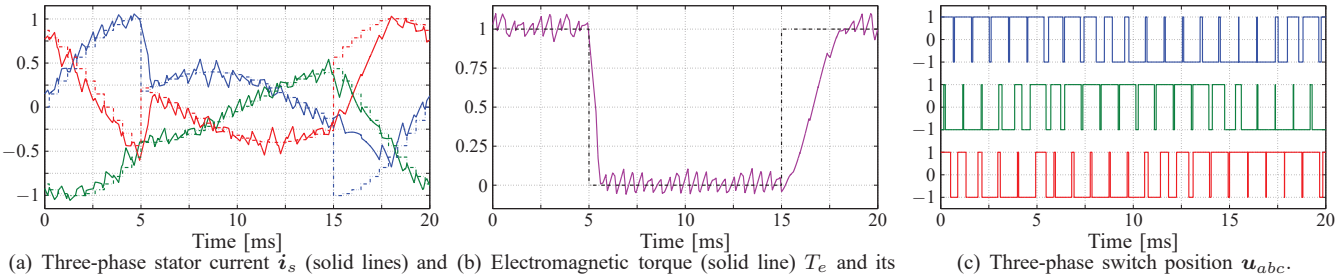

(a) Three-phase stator current $\boldsymbol{i}_s$ (solid lines) and their references (dash-dotted lines). (b) Electromagnetic torque (solid line) T_e and its reference (dash-dotted line). (c) Three-phase switch position $\boldsymbol{u}_{abc}$.

Fig. 6: Torque reference steps for direct MPC. The switching frequency is 1050 Hz.

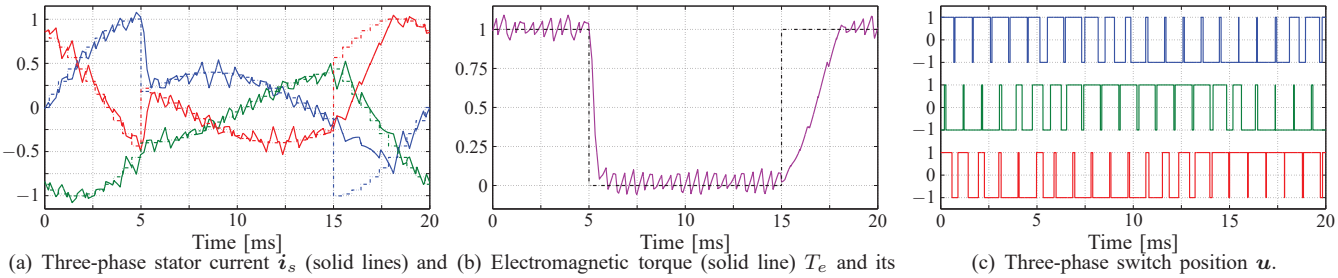

(a) Three-phase stator current $\boldsymbol{i}_s$ (solid lines) and their references (dash-dotted lines). (b) Electromagnetic torque (solid line) T_e and its reference (dash-dotted line). (c) Three-phase switch position $\boldsymbol{u}$.

Fig. 7: Torque reference steps for linear control with CB-PWM. The switching frequency is 1050 Hz.

[10] L. Tarisciotti, P. Zanchetta, A. Watson, J. C. Clare, M. Degano, and S. Bifaretti, "Modulated model predictive control for a three-phase active rectifier," *IEEE Trans. Ind. Appl.*, vol. 51, no. 2, pp. 1610–1620, Mar./Apr. 2015.

[11] Y. Zhang, Y. Peng, and C. Qu, "Model predictive control and direct power control for PWM rectifiers with active power ripple minimization," *IEEE Trans. Ind. Appl.*, vol. 52, no. 6, pp. 4909–4918, Nov./Dec. 2016.

[12] S. Aurtenechea Larrinaga, M. A. Rodríguez Vidal, E. Oyarbide, and J. R. Torrealday Apraiz, "Predictive control strategy for dc/ac converters based on direct power control," *IEEE Trans. Ind. Electron.*, vol. 54, no. 3, pp. 1261–1271, Jun. 2007.

[13] S. Vazquez, A. Marquez, R. Aguilera, D. Quevedo, J. I. Leon, and L. G. Franquelo, "Predictive optimal switching sequence direct power control for grid-connected power converters," *IEEE Trans. Ind. Electron.*, vol. 62, no. 4, pp. 2010–2020, Apr. 2015.

[14] W. Falmbigl, O. König, S. Jakubek, and G. Prochart, "Predictive pulse pattern control for a synchronous multiphase buck converter," in *Proc. Workshop on Pred. Control of Elect. Drives and Power Electron.*, Pilsen, Czech Republic, Sep. 2017, pp. 1–6.

[15] S. N. Manias, *Power electronics and motor drive systems*. Cambridge, MA: Academic Press, 2016.

[16] J. Holtz, "The representation of ac machine dynamics by complex signal flow graphs," *IEEE Trans. Ind. Electron.*, vol. 42, no. 3, pp. 263–271, Jun. 1995.